# Microscale Laser-Driven Particle Accelerator Using the Inverse Cherenkov Effect

Weihao Liu,[1,*] Zijia Yu,[2] Li Sun,[2] Yucheng Liu,[2] Qika Jia,[2] Hongliang Xu,[2] and Baogen Sun[2]

[1] *College of Electronic and Information Engineering, Nanjing University of Aeronautics and Astronautics, Nanjing, Jiangsu 211106, China*

[2] *National Synchrotron Radiation Laboratory, University of Science and Technology of China, Hefei, Anhui 230029, China*

(Received 28 January 2020; revised 3 March 2020; accepted 14 May 2020; published 7 July 2020)

We propose a microscale dielectric laser-driven particle accelerator based on the inverse effect of Cherenkov radiation. It utilizes a parallel-polarized laser beam that is incident perpendicularly on a right-angle surface of a high-breakdown-threshold prism, at the hypotenuse surface of which the laser-induced waves are innately synchronized with incoming free electrons, providing them with a continuous acceleration force. Compared with radio-frequency accelerators, its acceleration gradient is remarkably higher and its size is orders of magnitude smaller. In contrast to previous dielectric laser accelerators based on the inverse Smith-Purcell effect, it is not susceptible to the spectral dispersion of the laser pulse, and it can provide a long duration of the synchronized accelerating field without using external pulse-front-tilting techniques. In addition, it effectively avoids electron deflection caused by transverse fields, greatly improving the acceleration capability. Thus, it affords a promising way of developing ultracompact and highly efficient accelerators on chip.

DOI: 10.1103/PhysRevApplied.14.014018

## I. INTRODUCTION

The particle accelerator is one of the most important scientific instruments for the advancement of science and technology today [1]. However, conventional radio-frequency (rf) accelerators are generally large and expensive, and this has led to great efforts to develop compact and even tabletop particle accelerators during the past few decades [2,3]. Recently, the dielectric laser accelerator (DLA), which uses a high-power laser to drive a microscale dielectric structure with a high breakdown threshold, has attracted increasing interest, since it can potentially provide accelerating gradients of gigavolts per meter [4–7], significantly higher than conventional rf accelerators can provide using metallic structures. It shows promise for development into an ultracompact particle accelerator on chip [8].

Most of the available DLAs are based on the inverse Smith-Purcell effect [9–11], using a periodic dielectric structure to spatially modulate the incident laser field and synchronize the incoming free electrons with the spatial harmonics of the induced waves in the electron-beam channel [12–14]. The free electrons are alternately accelerated and decelerated along the channel; namely, they cannot be continuously accelerated, although they undergo a net acceleration in every period. In addition, external pulse-front-tilting techniques have to be applied in order to provide a long enough duration of the accelerating field [12,15]. Besides that, the transverse electromagnetic fields induced by the periodic boundaries cause the electrons to move toward or away from the structure, restricting the actual acceleration duration and the fraction of electrons accelerated [16,17]. Other DLAs resort to using slow-wave guided modes within photonic-band-gap structures [18,19] to provide a synchronized accelerating field. Unfortunately, they encounter the challenge of low coupling efficiency from the incident laser beam to the guided modes [20]. Also, the guided modes in the band-gap structures are essentially dispersive—waves of different frequencies have different phase velocities, such that only a certain part of the spectrum of the laser pulse can be synchronized with the electrons [8,20], greatly restricting the utilization efficiency of the laser pulse.

In the present paper, we propose a microscale dielectric laser-driven accelerator that is based on the inverse effect of the well-known Cherenkov radiation [21,22]. It synchronizes the electrons with the fundamental waves of the accelerating field, providing them with a continuous acceleration force without using external pulse-front-tilting techniques. In addition, it is nondispersive—waves with different wavelengths satisfy the same synchronization condition, which enhances the utilization efficiency of the laser pulse in consequence. Furthermore, it innately avoids electron deflection by counteracting the transverse

*liuwhao@nuaa.edu.cn

 

electric and magnetic forces, effectively improving the accelerating capability. Last but not least, it has a simple configuration and can be easily integrated on chip. Thus, it affords a promising way of developing ultracompact and highly efficient particle accelerators.

## II. PROPOSED SCHEME

A schematic illustration of the proposed scheme is shown in Fig. 1. It utilizes a parallel-polarized laser beam incident perpendicularly on a right-angle surface (surface I) of a high-breakdown-threshold prism with a right-triangle cross section. Free electrons move parallel to the hypotenuse surface (surface II) of the prism. The base angle ($\alpha$) of the prism, which is also the incidence angle of the laser beam on surface II, satisfies the relation

$$\sin\alpha = \frac{c/\sqrt{\varepsilon_r}}{v_z} = \frac{1}{\sqrt{\varepsilon_r}\beta_z}, \tag{1}$$

in which $\varepsilon_r$ is the relative permittivity of the prism, $v_z$ is the electron velocity in the $z$ direction, $c$ is the speed of light in vacuum, and $\beta_z = v_z/c$. The angle between the electron velocity and the incidence direction of the laser beam is $\theta = \pi/2 - \alpha$, as shown in the figure. According to Eq. (1), the incident laser beam is totally reflected at surface II, and the fields also penetrate through the surface, generating waves propagating along the surface with a phase velocity less than the speed of light in vacuum ($v_p < c$) [23], such that synchronization between the surface waves and the electrons can be realized. In the coordinate system shown in the figure, the electric fields of the incident and reflected waves at surface II can be decomposed into tangential ($z$ direction) and perpendicular ($x$ direction) components as follows:

$$E_0^{i,r} e^{jk_n^{i,r}R - j\omega t} = \left(E_x^{i,r}\hat{i}_x + E_z^{i,r}\hat{i}_z\right) e^{jk_x^{i,r}x + jk_z^{i,r}z - j\omega t}, \tag{2}$$

where $k_n^{i,r} = \sqrt{\varepsilon_r}\omega/c$ is the wave number in the dielectric prism, $\omega$ is the angular frequency, $(k_x^{i,r}, k_z^{i,r}) = k_n^{i,r}(\cos\alpha, \sin\alpha)$, $(E_x^i, E_z^i) = |E^i|(\sin\alpha, \cos\alpha)$, and $(E_x^r, E_z^r) = |E^r|(\sin\alpha, -\cos\alpha)$. $E^i$ and $E^r$ are the electric field intensities of the incident and reflected waves, respectively. The penetrating fields in the lower half-space can be obtained by solving the Maxwell equations [23,24]

$$(E_z^p, E_x^p, H_y^p) = (1, -jk_z^p/k_x^p, -j\omega\varepsilon/k_x^p) A_p e^{k_x^p x + jk_z^p z - j\omega t}, \tag{3}$$

where $A_p$ is a coefficient to be determined by use of the boundary conditions. Note that here all the field components of the penetrating wave decay exponentially away from surface II in the $-x$ direction, which is a typical feature of surface (evanescent) waves. The incident, reflected, and penetrating waves must satisfy the following boundary conditions:

$$\left[E_z^i + E_z^r\right]\big|_{x=0} = E_z^p\big|_{x=0}, \left[\varepsilon_r(E_x^i + E_x^r)\right]\big|_{x=0} = E_x^p\big|_{x=0}, \tag{4}$$

from which the field coefficient $A_p$ can be obtained in terms of the incident field as follows:

$$A_p \approx 2E^i \frac{\sqrt{\varepsilon_r}}{\gamma\beta_z}\left[1 - \frac{(\varepsilon_r\tan\alpha/\gamma)^2}{2}\right] e^{j\{\pi - \arctan[\gamma/(\varepsilon_r\tan\alpha)]\}}$$

(here $\gamma$ is the relativistic factor of the free electrons). Also, we can obtain the phase velocity of the surface wave along surface II, $v_p = \omega/k_z^p = \omega/(k_n^i\sin\alpha) = c/(\sqrt{\varepsilon_r}\sin\alpha) = v_z$; namely, the surface wave is synchronized with the free electrons in the $z$ direction. Note that here the synchronization is achieved without resorting to external pulse-front-tilting techniques, which are indispensable in previous DLAs based on inverse Smith-Purcell radiation (ISPR-DLAs).

Based on the field expressions in Eq. (3), we can evaluate the electromagnetic force exerted on a free-electron bunch, which is composed of three major parts: a longitudinal electric force, expressed as $F_{ez} = -q_e E_z^p$, a transverse electric force $F_{ex} = -q_e E_x^p$, and a transverse magnetic force $F_{mx} = q_e v_z \mu H_y^p$. Here $q_e$ is the quantity of charge in the electron bunch, which has a negative value, and $\mu$ is the permeability of the vacuum. The first part accelerates or decelerates the electrons, depending on the phase of the longitudinal field experienced by the electrons. The other two parts can deflect the electrons towards or away from surface II, as in previous DLAs. However, on examining these two transverse deflecting forces, we find that they are almost equal in magnitude and opposite in direction ($F_{mx} = -\beta_z^2 F_{ex} \approx -F_{ex}$), indicating that the transverse electric and magnetic forces largely counteract each other, such that the electron deflection is effectively restricted, which is an innate advantage of the proposed scheme.

We note further that synchronization between the free electrons and the accelerating field can be achieved in

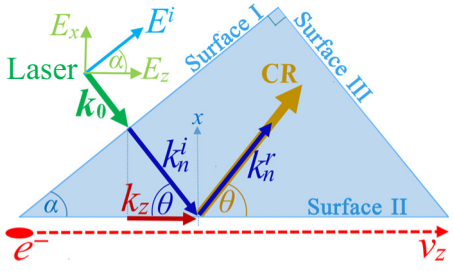


FIG. 1. Two-dimensional schematic diagram of the proposed particle accelerator. The yellow arrow denotes the direction of the Cherenkov radiation (CR).

the proposed scheme provided that the electron velocity is greater than the speed of light in the prism ($v_z > c/\sqrt{\varepsilon_r}$), which is exactly the requirement for Cherenkov radiation [25]. Also, the angle between the incidence direction of the laser beam and the electron velocity is equal to the Cherenkov angle, which can be expressed as $\theta = \arccos\left(1/\sqrt{\varepsilon_r}\beta_z\right)$; see Fig. 1. From the perspective of energy transformation, the electrons lose energy and are decelerated due to the radiation loss associated with the CR. In contrast, the electrons gain energy from the laser field and are accelerated in the present scheme; in other words, the particle acceleration and CR are essentially two inverse physical mechanisms. Hereinafter, we call the proposed accelerator an inverse-Cherenkov-radiation DLA (ICR-DLA), analogously to the ISPR-DLA. According to Eq. (1), the synchronization condition for an ICR-DLA is wavelength independent (nondispersive), following the CR relation, in which the radiation direction is independent of the wavelength. In other words, laser fields with different wavelengths can be used in the same ICR-DLA model. In contrast, the ISPR-DLA is wavelength dependent (dispersive), since Smith-Purcell radiation is innately dispersive: waves with different wavelengths are radiated in different directions. We would like to mention that the proposed ICR-DLA also has obvious advantages over previous inverse-CR accelerators (ICAs), which use gases to slow the laser waves [26,27], since the breakdown threshold of a dielectric medium can be much higher than that of a dense gas, and microscale dielectric (solid-sate) structures are quite compact and are easy to integrate on chip.

## III. SIMULATIONS AND DISCUSSIONS

In the following, we carry out calculations and simulations for the proposed scheme. As an example, the initial electron energy is set to 10 MeV, and a $CO_2$ laser beam with a wavelength of 10 $\mu$m is used to drive the prism. The prism is chosen to be made of high-breakdown-threshold quartz with a refractive index $n = \sqrt{\varepsilon_r} = 1.548$, and the base angle is $\alpha = 40.2^\circ$, satisfying Eq. (1). The hypotenuse length of the prism is 200 $\mu$m, and the thickness of the prism in the $y$ direction is 100 $\mu$m. In the simulations, we first use an electromagnetic code [28] to obtain the field distributions in and around the prism. A simulated contour map of the component $E_z$ is illustrated in Fig. 2(a), which clearly shows that the phase velocity $v_p$ of the wave along surface II is $c/(n\sin\alpha)$, matching the electron velocity. The field patterns within the prism are formed by interference of the incident and reflected waves. The simulated and calculated results for the normalized component $E_z$ along surface II are illustrated in Fig. 2(b). We note that the simulated field-oscillation period in the $z$ direction, which determines the longitudinal phase velocity $v_p$, largely agrees with the theoretical value in the front part of the electron path (before $z \approx 180$ $\mu$m). However, it deviates from the theoretical result in the later part (after $z \approx 180$ $\mu$m). This may be due to reflection at the other right-angle surface (surface III) and diffraction at the prism corners, which are not taken into considerations in the analytic calculations. It is worth mentioning that although free-space excitation is illustrated here, a similar scheme can easily be integrated with photonic circuits on chip, since there is no requirement for external pulse-front-tilting equipment.

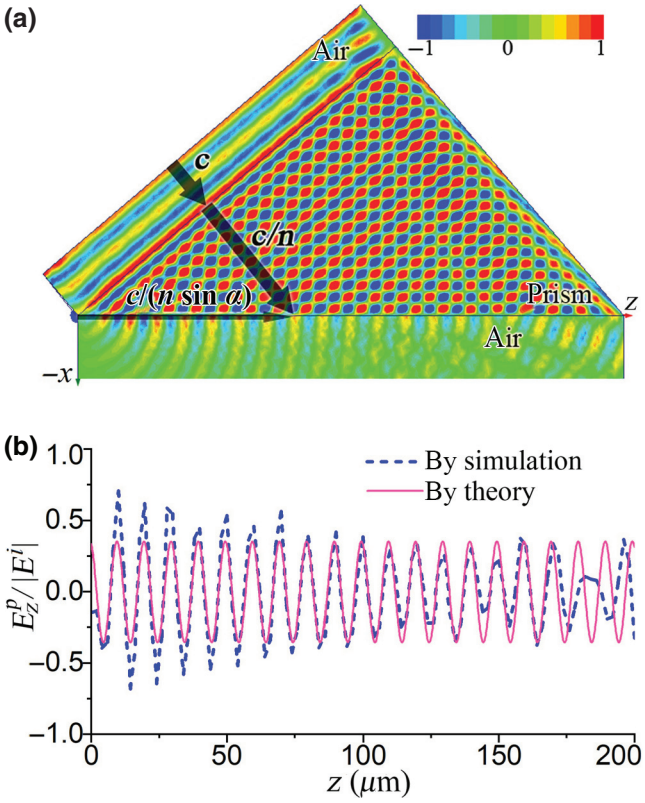


FIG. 2. (a) Simulated contour map of the component $E_z$. Here $c$, $c/n$, and $c/(n\sin\alpha)$ denote the phase velocities of the waves in vacuum, in the prism, and along surface II, respectively. (b) Simulated and calculated components $E_z$ (normalized to the incident field intensity $E^i$) along surface II in the $z$ direction.

The simulated electromagnetic fields (including all field components), multiplied by a specified scaling factor signifying the intensity of the incident laser beam, are then input into the code General Particle Tracer (GPT) [29] to simulate the electron dynamics. In the simulations, the injected electron bunch is composed of 5000 macroparticles, which follow Gaussian distributions in both the longitudinal and the transverse (radial) direction within the bunch. The total charge of the bunch is set to 1 fC, and the space-charge effect is taken into consideration by using the Poisson equation and the Lorentz transformation [29]. The initial transverse rms bunch size (radius) is set to 0.2 $\mu$m, and the initial transverse emittance $\epsilon_n$ is $10^{-9}$ m rad. The distance $h$ from the bunch center to surface II is 3 $\mu$m. The

longitudinal bunch length is 0.3 $\mu$m, corresponding to a time duration of 1 fs, which is much less than the time period of the laser field, so that all electrons in the bunch experience largely the same accelerating field at the beginning. In practice, the initial phase of the laser field can be optimized to obtain the desired electron acceleration. The electric field intensity $E^i$ of the incident laser beam is set to 5 GV/m, implying that the power density of the laser beam is about $6.6 \times 10^{12}$ W/cm$^2$ [30]. Assuming that the accelerating field is synchronized with the electron bunch, a single-cycle laser pulse can provide sufficient acceleration for the electron bunch all the way along the electron path, so that the energy density of the laser pulse illuminating the prism can be evaluated by multiplying the power density by the pulse duration (approximately 30 fs), giving a value of about 0.2 J/cm$^2$. This is much less than the breakdown threshold of quartz, which can be greater than 1 J/cm$^2$ according to previous studies [31,32]; in other words, the laser field used in our simulations is acceptable in practice, since it will not damage the prism.

Figure 3(a) shows the longitudinal electric field ($E_z$) experienced by the electron bunch. Here and in Figs. 3(b)–(d), simulated results at different positions in the $z$ direction are shown together to illustrate the evolution in the longitudinal direction of the fields experienced by the electrons and that of the bunch parameters. We note that the field $E_z$ experienced by the electron bunch is always negative, indicating that the longitudinal electric force exerted on the bunch is always positive ($F_{ez} > 0$), so that the bunch is continuously accelerated. The fluctuations of the fields, especially around the two ends, are due to the nonuniformities of the fields around the corners of the prism mentioned previously. The field components $E_x$ and $B_y$ experienced by the electron bunch are shown in Fig. 3(b), which illustrates that their amplitudes change simultaneously; in other words, their phases follow the same variation function (they are in phase). Calculations show that the transverse electric and magnetic forces (in the $x$ direction) exerted on the electrons are nearly equal in magnitude and opposite in direction. The electron trajectories in the $x$-$z$ plane are observed in Fig. 3(c), which illustrates that the deflection of the electrons in the $x$ direction is quite small (less than 0.3 $\mu$m), indicating that the transverse deflection forces largely counteract each other, agreeing with the theoretical prediction. The insets show that the transverse size of the electron bunch does not change very much from the beginning to the end. Figure 3(d) shows that both the electron energy (represented by $\gamma$) and the longitudinal velocity (represented by $\beta_z$) increase gradually in the $z$ direction as expected. The calculated average acceleration gradient (AAG) is about 1.5 GV/m, obtained by dividing the total energy gain of an electron ($\Delta\gamma \approx 0.6$, corresponding to $\Delta_e \approx 0.3$ MeV) by the whole path length (200 $\mu$m). We note that the acceleration gradient shows an obvious decrease in the rear part of the electron path.

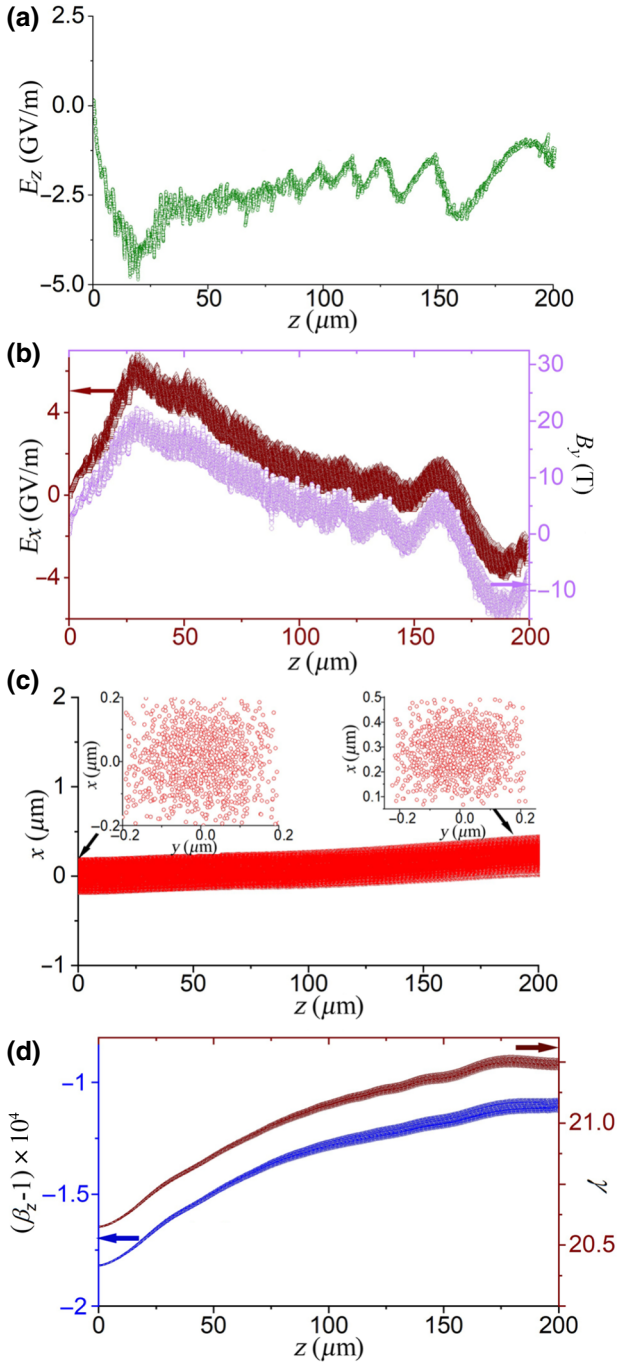


FIG. 3. (a) Field component $E_z$ experienced by electrons along the electron path. (b) Field components $E_x$ and $B_y$ experienced by electrons along the electron path. (c) Electron trajectories in the $x$-$z$ plane. The insets show the transverse bunch sizes at the front and rear ends. (d) Relativistic factors $\gamma$ and $\beta_z$ of the electrons versus electron position in the $z$ direction.

This is because the field distributions in the rear part are distorted away from the ideal distributions, as shown in Fig. 2(b), and because the synchronization condition is not perfectly satisfied in the rear part, due to the acceleration of the electrons as indicated in Fig. 3(a). Based on

the above simulation results, we can evaluate the accelerating efficiency of the proposed ICR-DLA, namely, the fraction of the laser energy that is transformed into kinetic energy of the electron bunch. Since the actual utilized area of the laser pulse incident on surface I is approximately 75 $\mu m^2$ [33], the utilized energy of the laser pulse is about $1.5 \times 10^{-7}$ J. Dividing this by the total energy gain of the electron bunch, which is $\Delta_K = N_e \Delta_e \approx 3 \times 10^{-10}$ J (where $N_e$ is the number of electrons in the bunch), we find that the energy efficiency is approximately $2 \times 10^{-3}$. It should be noted that, along with acceleration of the electrons, wakefield radiation (i.e., CR) is also generated by the electron bunch in the prism, since the CR condition is satisfied, and this can decelerate the electron bunch via radiation loss. This radiation loss is not taken into consideration in the GPT simulations. Based on previous investigations [34], we find that it is insignificant in the present model, since a low-charge electron bunch is used.

Figure 4(a) shows that the AAG decreases exponentially as the distance from the bunch center to surface II ($h$) increases. This can be understood from the fact that the electron bunch is synchronized with the evanescent wave, in which the fields decay exponentially away from the surface as mentioned previously. Figure 4(b) illustrates that both the energy spread and the normalized transverse emittance increase gradually as the electron bunch moves in the $z$ direction. This is also because of the nonuniform distribution of the fields along the electron path mentioned previously. Thus, the transverse size of the electron bunch,

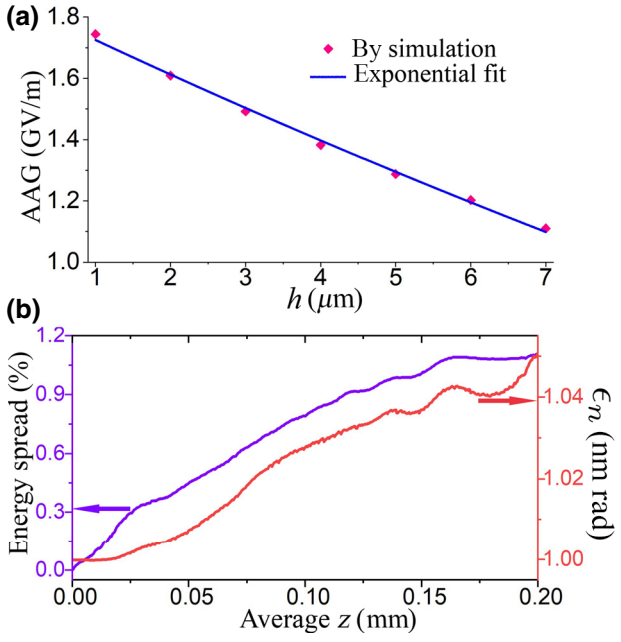


FIG. 4. (a) Simulated AAG as a function of $h$, and exponential fit. (b) Simulated energy spread and transverse emittance ($\epsilon_n$) of an electron bunch versus bunch position in the $z$ direction.

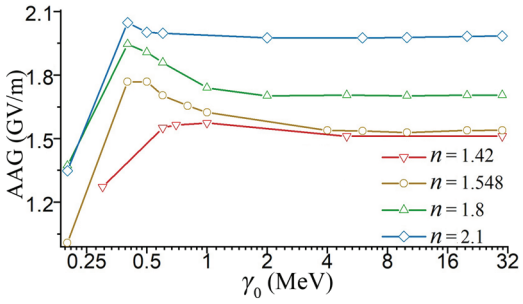


FIG. 5. Average acceleration gradient as a function of the initial electron energy $\gamma_0$ and of the refractive index $n$ of the prism.

as well as the value of $h$, needs to be well chosen in practice.

To illustrate the acceleration capability of the proposed scheme, we gradually change the initial electron energy ($\gamma_0$) together with the refractive index $n$ of the prism, while keeping the synchronization condition of Eq. (1). The simulated AAGs are presented in Fig. 5, which shows that the AAG increases as $n$ increases and that, for each value of $n$, the AAG first increases and then decreases as $\gamma_0$ increases; namely, there is an optimum $\gamma_0$ (or maximum AAG) for each material. This can be understood from the fact that for a fixed $\gamma_0$, a larger $n$ means a smaller $\alpha$, which leads to a greater longitudinal accelerating field $E_z$ according to Eq. (2). If, instead, $n$ is specified, when $\gamma_0$ is relatively small (i.e., for subrelativistic electrons), a larger electron energy means a larger $\beta_z$ and a smaller $\alpha$, which leads to a greater acceleration gradient as mentioned. If $\gamma_0$ is large enough (i.e., for relativistic electrons), $\beta_z$ (together with $\alpha$) almost does not change with $\gamma_0$, and the electric field of the electrons is largely in the transverse direction, which restricts the longitudinal accelerating gradient. We note that the AAG, together with $\alpha$, almost does not change if $\gamma_0$ is large enough, indicating that a single prism can be used to accelerate relativistic electrons with a wide range of energies. In practice, an array of cascaded prisms, driven by an array of phase- and amplitude-manipulated laser beams [35], can be utilized to provide the electrons with continuous acceleration fields from subrelativistic to relativistic states.

## IV. CONCLUSIONS

In conclusion, we propose and investigate a microscale particle accelerator using high-power laser pulses to drive a high-breakdown-threshold dielectric prism. In principle, it is based on the inverse effect of Cherenkov radiation, and is essentially different from previous dielectric laser accelerators, which are based on the inverse Smith-Purcell effect. It can provide a synchronized acceleration field without using external pulse-front-tilting techniques, and it innately avoids electron deflection caused by transverse electric and magnetic fields. Detailed analyses of

the requirements and the main properties of this particle accelerator are performed, and the acceleration efficiency is evaluated. It is a promising candidate for ultracompact and highly efficient accelerators on chip.

## ACKNOWLEDGMENTS

This work was supported by the Natural Science Foundation of China (Grants No. U1632150, No. 61471332, and No. 11675178).

[1] D. A. Edwards and M. J. Syphers, *An Introduction to the Physics of High Energy Accelerators* (WILEY-VCH Verlag GmbH and Co. KGaA, Morlenbach, 2004).

[2] B. Neuner III, D. Korobkin, G. Ferro, and G. Shvets, Prism-coupled surface wave accelerator based on silicon carbide, Phys. Rev. Spec. Top. Accel. Beams **15**, 031302 (2012).

[3] A. Mizrahi and L. Schachter, Optical Bragg accelerators, Phys. Rev. E **70**, 016505 (2004).

[4] J. B. Rosenzweig, A. Murokh, and C. Pellegrini, A Proposed Dielectric-Loaded Resonant Laser Accelerator, Phys. Rev. Lett. **74**, 2467 (1995).

[5] E. A. Peralta, K. Soong, R. J. England, E. R. Colby, Z. Wu, B. Montazeri, C. McGuinness, J. McNeur, K. J. Leedle, D. Walz, E. B. Sozer, B. Cowan, B. Schwartz, G. Travish, and R. L. Byer, Demonstration of electron acceleration in a laser-driven dielectric microstructure, Nature **503**, 91 (2013).

[6] J. Breuer and P. Hommelhoff, Laser-Based Acceleration of Nonrelativistic Electrons at a Dielectric Structure, Phys. Rev. Lett. **111**, 134803 (2013).

[7] R. J. England *et al.*, Dielectric laser accelerator, Rev. Mod. Phys. **86**, 1337 (2014).

[8] N. V. Sapra, K. Y. Yang, D. Vercruysse, K. J. Leedle, D. S. Black, R. J. England, L. Su, R. Trivedi, Y. Miao, O. Solgaard, R. L. Byer, and Jelena Vuckovic, On-chip integrated laser-driven particle accelerator, Science **367**, 79 (2020).

[9] K. Mizuno, S. Ono, and O. Shimoe, Interaction between coherent light waves and free electrons with a reflection grating, Nature **253**, 184 (1975).

[10] J. Bae, H. Shirai, T. Nishida, T. Nozokido, K. Furuya, and K. Mizuno, Experimental verification of the theory on the inverse Smith–Purcell effect at a submillimeter wavelength, Appl. Phys. Lett. **61**, 870 (1992).

[11] J. Breuer and P. Hommelhoff, Dielectric laser acceleration of 28 keV electrons with the inverse Smith–Purcell effect, Nucl. Instrum. Methods Phys. Res. A **740**, 114 (2014).

[12] Y. Wei, G. Xia, J. D. A. Smithe, K. Hanahoea, O. Metea, S. P. Jamisona, and C. P. Welsch, Numerical study of a multi-stage dielectric laser-driven accelerator, Phys. Procedia **77**, 50-57 (2015).

[13] B. Naranjo, A. Valloni, S. Putterman, and J. B. Rosenzweig, Stable Charged-Particle Acceleration and Focusing in a Laser Accelerator Using Spatial Harmonics, Phys. Rev. Lett. **109**, 164803 (2012).

[14] J. Breuer, R. Graf, A. Apolonski, and P. Hommelhoff, Dielectric laser acceleration of nonrelativistic electrons at a single fused silica grating structure: Experimental part, Phys. Rev. Spec. Top. Accel. Beams **17**, 021301 (2014).

[15] K. P. Wootton, Z. Wu, B. M. Cowan, A. Hanuka, I. V. Makasyuk, E. A. Peralta, K. Soong, R. L. Byer, and J. R. England, Demonstration of acceleration of relativistic electrons at a dielectric microstructure using femtosecond laser pulses, Opt. Lett. **41**, 2696 (2016).

[16] K. J. Leedle, R. F. Pease, R. L. Byer, and J. S. Harris, Laser acceleration and deflection of 96.3 keV electrons with a silicon dielectric structure, Optica **2**, 158 (2015).

[17] In previous DLAs based on the inverse Smith-Purcell effect, even though the transverse deflecting field and the longitudinal accelerating field are out of phase, deflection of the electron bunch is unavoidable, since the electron bunch extends over a certain range of phases and only a small fraction of the electrons can avoid deflection.

[18] X. E. Lin, Photonic band gap fiber accelerator, Phys. Rev. Spec. Top. Accel. Beams **4**, 051301 (2001).

[19] B. M. Cowan, Three-dimensional dielectric photonic crystal structures for laser-driven acceleration, Phys. Rev. Spec. Top. Accel. Beams **11**, 011301 (2008).

[20] R. J. England, A. Kwiatkowski, C.-K. Ng, and Z. Wu, Input coupling for photonic bandgap fiber accelerators, IEEE J. Sel. Top. Quant. Elect. **22**, 4401109 (2016).

[21] P. A. Cherenkov, Visible radiation produced by electrons moving in a medium with velocities exceeding that of light, Phys. Rev. **52**, 378 (1937).

[22] B. M. Bolotovskii, Vavilov-Cherenkov radiation: Its discovery and application, Phys. Usp. **52**, 1099 (2009).

[23] H. Raether, *Plasmons on Smooth and Rough Surfaces and on Gratings* (Springer-Verlag, Berlin, 1988).

[24] K. Zhang and D. Li, *Electromagnetic Theory in Microwave and Optoelectronics* (Springer-Velag, Berlin, 2008).

[25] J. D. Jackson, *Classical Electrodynamics* (Wiley, Hoboken, 1997).

[26] J. R. Fontana and R. H. Pantell, Electron momentum modulation by the stimulated Cerenkov interaction, J. Appl. Phys. **53**, 5435 (1982).

[27] W. D. Kimura, G. H. Kim, R. D. Romea, L. C. Steinhauer, I. V. Pogorelsky, K. P. Kusche, R. C. Fernow, X. Wang, and Y. Liu, Laser Acceleration of Relativistic Electrons Using the Inverse Cherenkov Effect, Phys. Rev. Lett. **74**, 547 (1995).

[28] CST Corp., CST PS Tutorials, http://www.cstchina.cn/.

[29] General Particle Tracer (GPT), Pulsar Physics, http://www.pulsar.nl/.

[30] The power density can be obtained from $P^i = |E^i|^2/\eta$, where $\eta$ is the wave impedance in vacuum.

[31] M. Lenzner, J. Kruger, S. Sartania, Z. Cheng, C. Spielmann, G. Mourou, W. Kautek, and F. Krausz, Femtosecond Optical Breakdown in Dielectrics, Phys. Rev. Lett. **80**, 4076 (1998).

[32] Ken Soong, R. L. Byer, E. R. Colby, R. J. England, and E. A. Peralta, Laser damage threshold measurements of optical materials for direct laser accelerators, AIP Conf. Proc. **1507**, 511 (2012).

[33] The transverse shape of the laser pulse incident on surface I can be approximated by a rectangle with a side length of approximately 150 $\mu$m in the parallel direction, which is the length of the right-angle side of the cross section of the prism, and with a side length of approximately 0.5 $\mu$m

in the perpendicular direction, which is approximately the bunch size in the $y$ direction.

[34] S. Liu, P. Zhang, W. Liu, S. Gong, R. Zhong, Y. Zhang, and M. Hu, Surface Polariton Cherenkov Light Radiation Source, Phys. Rev. Lett. **109**, 153902 (2012).

[35] T. Hughes, S. Tan, Z. Zhao, N. Sapra, K. Leedle, H. Deng, Y. Miao, D. Black, O. Solgaard, J. Harris, J. Vuckovic, R. Byer, S. Fan, R. England, Y. J. Lee, and M. Qi, On-Chip Laser-Power Delivery System for Dielectric Laser Accelerators, Phys. Rev. Appl. **9**, 054017 (2018).